Wireless Energy Transmission Channel Modeling in Resonant Beam Charging for IoT Devices

Wei Wang, Qingqing Zhang, Hua Lin, Mingqing Liu, Xiaoyan Liang, and Qingwen Liu

***Abstract*—Power supply for Internet of Things (IoT) devices is one of the bottlenecks in IoT development. To provide perpetual power supply for IoT devices, resonant beam charging (RBC) is a promising safe, long-range, and high-power wireless power transfer solution. How long distance RBC can reach and how much power RBC can transfer? In this paper, we analyze the consistent and steady operational conditions of the RBC system, which determine the maximum power transmission distance. Then, we study the power transmission efficiency within the operational distance, which determines the deliverable power through the RBC energy transmission channel. Based on the theoretical model of the wireless energy transmission channel, we establish a testbed. According to the experimental measurement, we validate our theoretical model. The experiments verify that the output electrical power at the RBC receiver can be up to 2 W. The maximum energy transmission distance is 2.6 m. Both the experimental and theoretical performance of the RBC system are evaluated in terms of the transmission distance, the transmission efficiency, and the output electrical power. Our theoretical model and experimental testbed lead to the guidelines for the RBC system design and implementation in practice.**

***Index Terms*—Energy transmission channel modeling, experimental testbed, resonant beam charging (RBC), wireless power transfer (WPT).**

I. Introduction

With the development of Internet of Things (IoT) [1]–[3] and the big data [4], the power supply for IoT devices has become one of the bottlenecks of IoT development. However, carrying a power cord and looking for the power supply cause inconvenience for people. The contradiction between battery endurance of IoT devices and the power supply is increasingly prominent [5]–[8]. Therefore, wireless power transfer (WPT) draws much attention to provide mobile power supply anywhere and anytime for IoT devices.

Manuscript received June 4, 2018; revised December 8, 2018; accepted January 4, 2019. Date of publication January 18, 2019; date of current version May 8, 2019. *(Wei Wang and Qingqing Zhang contributed equally to this work.) (Corresponding authors: Xiaoyan Liang; Qingwen Liu.)*

W. Wang is with the State Key Laboratory of High Field Laser Physics, Shanghai Institute of Optics and Fine Mechanics, Chinese Academy of Sciences, Shanghai 201800, China, and also with the Center of Materials Science and Optoelectronics Engineering, University of Chinese Academy of Sciences, Beijing 100049, China (e-mail: wangwei2016@siom.ac.cn).

Q. Zhang, M. Liu, and Q. Liu are with the College of Electronic and Information Engineering, Tongji University, Shanghai 201804, China (e-mail: anne@tongji.edu.cn; 18392105294@163.com; qliu@tongji.edu.cn).

H. Lin and X. Liang are with the State Key Laboratory of High Field Laser Physics, Shanghai Institute of Optics and Fine Mechanics, Chinese Academy of Sciences, Shanghai 201800, China (e-mail: hual@siom.ac.cn; liangxy@siom.ac.cn).

Digital Object Identifier 10.1109/JIOT.2019.2894008

Several kinds of WPT technologies have been well investigated in research [9]. Inductive coupling [10] is safe and simple but limited by a short charging distance from a few millimeters to centimeters. Magnetic resonance coupling [11] has high charging efficiency. However, it is restricted by a short charging distance and a large coil size. Radio frequency [12] has a long effective charging distance. However, it suffers low efficiency and is difficult to balance safety and high power. Laser charging [13], [14] needs directional pointing and can transmit high power to a long distance. But it also faces the radiation safety challenge. In summary, these technologies face technical challenges to satisfy safety, long-range, and high-power at the same time.

Resonant beam charging (RBC), also known as distributed laser charging, is presented in [15] and [16], which can safely provide multi-Watt wireless power supply over multimeter distance for IoT devices. In the RBC system, any object blocking the line of sight between the transmitter and the receiver can break resonation immediately, which leads to the inherent safety. Meanwhile, when the RBC system operates as a stable resonant cavity, even slight blocking of the beam will instantly cause a significant alteration in the beam's power, which makes it simple to detect such a blocking. Furthermore, bystanders outside the resonant cavity limits will not be exposed to the resonant beam radiation. Moreover, the RBC supports self-aligning and simultaneous multidevices charging. To improve the WPT efficiency, the adaptive RBC system is proposed with the feedback control in [17] and [18].

Fig. 1 illustrates the potential RBC application. As shown, the RBC transmitter can be mounted on a communication base station to provide wireless power for the devices within its coverage. In addition, the unmanned aerial vehicle (UAV) equipped with both the RBC transmitter and receiver can play the role of a relay to receive power from the transmitter and transmit power to IoT devices within its coverage.

RBC is a promising solution to break the power supply bottleneck in development of IoT. However, how long distance RBC can reach and how much power RBC can transfer are essential issues to investigate. The contributions of this paper include the following.

1) We present the analytical model of the RBC energy transmission channel and analyze the RBC's consistent and steady operating conditions and the power transmission efficiency within the operational distance.
2) We establish an RBC testbed which can deliver up to 2 W electrical power from the transmitter to the receiver, and the maximum energy transmission distance is 2.6 m.

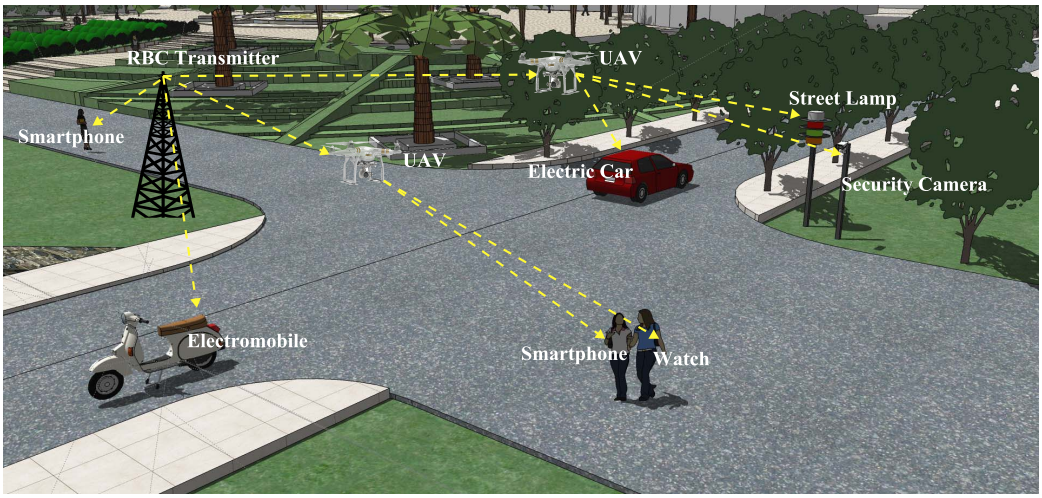

Fig. 1. RBC application.

3) Based on the experimental measurement, we validate our theoretical model. We further evaluate the RBC system performance by both theoretical analysis and experimental tests.

In the rest of this paper, we will briefly introduce the RBC system at first. Then, we will give the modular model and working mechanism of the RBC system. In the following, we will introduce the testbed of the RBC system, and evaluate the RBC system performance according to both the measured and simulated data. Finally, we will make conclusions and discuss open issues for future research.

II. RBC

The RBC is a WPT technology which transfers power through the intracavity resonant beam. In the RBC system, the optical components are divided into two separate parts: 1) the transmitter and 2) the receiver. The architecture of the RBC system is shown in Fig. 2. In the RBC transmitter, there is a high reflectivity curved mirror M1 and a gain medium pumped by pump source. The pump source excites gain medium to realize population inversion, which leads to energy storage in the gain medium. The energy stored in the gain medium is determined by the input electrical power, the performance of pump source, the pump chamber structure, and the property of gain medium [19].

In the RBC receiver, a partially transparent curved mirror M2 is taken to set up the optical resonant cavity with the mirror M1. The resonant cavity is a highly selective reflecting element. If the reflectivity of the resonant cavity is large enough to compensate for the internal losses, the system starts to oscillate when being triggered by the spontaneous radiation emitted along the axis of the resonant cavity. To guarantee RBC transmission efficiency, the reflectivity of M1 and M2 should be large enough so that the resonant cavity should be in the stability condition. Only the stability condition is satisfied, can high safety and efficiency of the resonant cavity be guaranteed. Under the stability condition, the gain medium stored energy is stimulated out to form the intracavity resonant beam [19]. The intracavity resonant beam partially leaks out from M2 and forms the external-cavity beam.

The intracavity resonant beam emitted by the general optical resonant cavity contains several discrete optical frequencies. The beams differ from each other with the beam frequency. The frequency differences can lead to different modes of the optical resonant cavity. Each mode is defined by the variation of the electromagnetic field perpendicular and along the axis of the resonant cavity. It is common to distinguish two types of resonant cavity modes: 1) longitudinal modes and 2) transverse modes. Each longitudinal mode is with a unique oscillation frequency. While the transverse mode is distinguished by the oscillation frequency and the field distribution perpendicular to the direction of propagation [19].

The internal losses affect the gain medium stored energy to the external-cavity beam power transmission efficiency. There are two kinds of loss with different properties in the RBC system [20]. The first kind is the loss independent of the resonant beam transverse mode, such as the scattering, absorption, and transmission losses. The scattering and absorption losses are caused by a variety of the system components, while the transmission loss is caused by the mirror. The other kind is the diffraction loss that closely related to the transverse mode and the transmission distance.

In the RBC receiver, a photovoltaic panel (PV-panel) is installed behind the mirror M2. The external-cavity beam power can be converted to electrical power by the PV-panel. The beam power-to-electrical power conversion is based on the PV engineering [21]–[23]. The factors affecting the end-to-end power transmission efficiency will be described in detail in the next section.

III. Analytical Model

In the RBC system, the input electrical power will be converted to the gain medium stored energy. Then, the gain medium stored energy will be converted to the intracavity resonant beam power, which will be transmitted from the transmitter to the receiver over a certain distance. Then, the

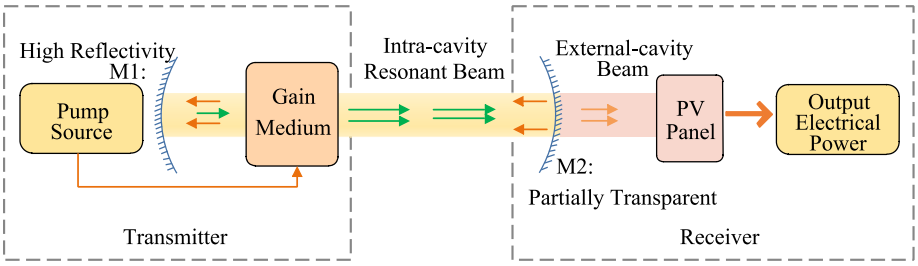

Fig. 2. RBC system.

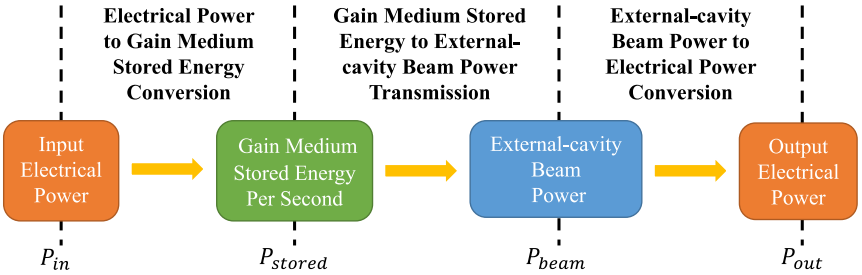

Fig. 3. RBC modular model.

intracavity resonant beam power will be partially converted to the external-cavity beam power in the receiver. Finally, the external-cavity beam power will be converted to the output electrical power, which can be used to charge devices accessed to the RBC system.

In this section, we will illustrate the analytical model of the RBC energy transmission channel by dividing the procedure into three stages: 1) the input electrical power to the gain medium stored energy conversion; 2) the gain medium stored energy to the external-cavity beam power transmission; and 3) the external-cavity beam power to the output electrical power conversion. Fig. 3 gives the modular model and the three energy transmission stages of the RBC system.

A. Electrical Power-to-Stored Energy Conversion

The input electrical power P_{in}, which is provided by the driving source, acts on the pump source. The pump source transforms the electrical power into the pump power which can be absorbed by the gain medium. Then, the pump power is transferred to the gain medium through a completely enclosed reflective chamber, i.e., pump chamber. The absorbed pump power excites the gain medium to realize the population inversion, and then the energy is stored in the gain medium.

In the case of continuous input of electrical power, the relationship between the gain medium stored energy per second P_{stored} and the input electrical power P_{in} can be depicted as [19]

$$P_{\text{stored}} = \eta_{\text{stored}} P_{\text{in}} \tag{1}$$

where η_{stored} is the electrical power-to-stored energy conversion efficiency. It is affected by the performance of the pump source, the pump chamber structure, and the material and size of gain medium [19]. η_{stored} can be computed as

$$\eta_{\text{stored}} = \frac{P_{\text{stored}}}{P_{\text{in}}}. \tag{2}$$

Most of the input electrical power that cannot be converted to the stored energy will dissipate as heat.

B. Stored Energy-to-Beam Power Transmission

The stored energy in the transmitter can be triggered by the spontaneous radiation emitted along the axis of the resonant cavity, and be converted to the intracavity resonant beam power. After part of the intracavity resonant beam passing through the partially transparent mirror M2, the external-cavity beam is formed. Therefore, with the transmission attenuation in the free space, the stored energy will be converted into the external-cavity beam power. Since both the transmission distance and the transmission efficiency have effects on the stored energy to beam power transmission efficiency, we will give the transmission distance model at first. Then, we will analyze the factors which influence the transmission efficiency.

1) Transmission Distance Modeling: To support the energy transmission, the resonant cavity should keep stable at first. Factors that influence the stability condition include the material and structure of the gain medium, the curvature radius of the mirror in the transmitter M1 and that of the mirror in the receiver M2, the distance between the gain medium and M1 l, and the distance between the gain medium and M2 d.

A resonant cavity containing a rod-shaped gain medium is taken as an example. In the rod, the heat generation is uniform, which acts as a lens-like medium due to thermal and stress-induced effects. From [24], the resonant cavity can be represented by a model containing a thin lens, as shown in Fig. 4. Where the gain medium is replaced by a thin lens with a focal length of f, $R1$ is the curvature radius of M1 mirror, $R2$ is the curvature radius of M2 mirror, l represents the space size of the transmitter, and d represents the transmission distance. We define the effective resonant cavity length L as

$$L = l + d - \frac{ld}{f}. \tag{3}$$

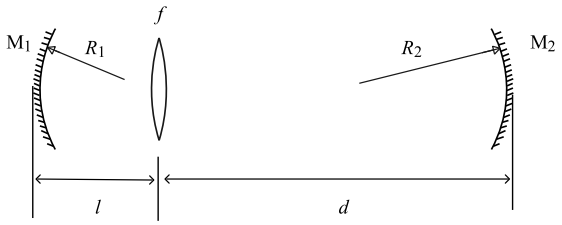

Fig. 4. Schematic of resonant cavity with thermal lens.

To express the stability condition of the resonant cavity more clearly, we introduce g_1, g_2 as

$$g_1 = 1 - \frac{d}{f} - \frac{L}{R_1} \tag{4}$$

$$g_2 = 1 - \frac{l}{f} - \frac{L}{R_2}. \tag{5}$$

As can be seen, g_1 and g_2 are both related to the transmission distance d. According to [25], to keep the RBC system working at the stability condition, the following condition should be satisfied:

$$0 < g_1 g_2 < 1. \tag{6}$$

To show graphically which type of resonant cavity is stable and which is unstable, it is useful to plot a stability diagram Fig. 5. In Fig. 5, each particular resonant cavity geometry is represented by a point to show the stable or unstable resonant cavity type. All cavity configurations are unstable unless they correspond to points located in the area enclosed by a branch of the hyperbola $g_1 g_2 = 1$ and the coordinate axes, as shown in the shadow part of Fig. 5. As the distance d varies, the straight line in Fig. 5 is derived by eliminating d in (4) and (5)

$$g_2 = \frac{(l-f)R_1}{(l-R_1-f)R_2} g_1 + \frac{(l-f)(l-R_1)}{(l-R_1-f)R_2} + 1 - \frac{l}{f} - \frac{l}{R_2}. \tag{7}$$

The two straight lines in Fig. 5 correspond to two general situations. The intersections of the straight line with the axes and with the hyperbola $g_1 g_2 = 1$ determine the critical values of d corresponding to the edges of the stability regions [26]. In our theoretical model, the range of d satisfying the stability condition represents the distance range that can realize energy transmission. The critical value of d determines the maximum transmission distance of the RBC system.

Though the intensity distribution on each section of the resonant beam is consistent, the beam radius (defined as the radius at which the electric field amplitude is down by $1/e$ from the maximum) of the intensity distribution varies along the optical axis [19]. For analyzing the relationship between the beam radius of each location and the transmission distance more concisely, we introduce three new variables u_1, u_2, and x as

$$u_1 = l\left(1 - \frac{l}{R_1}\right) \tag{8}$$

$$u_2 = d\left(1 - \frac{d}{R_2}\right) \tag{9}$$

$$x = \frac{1}{f} - \frac{1}{l} - \frac{1}{d}. \tag{10}$$

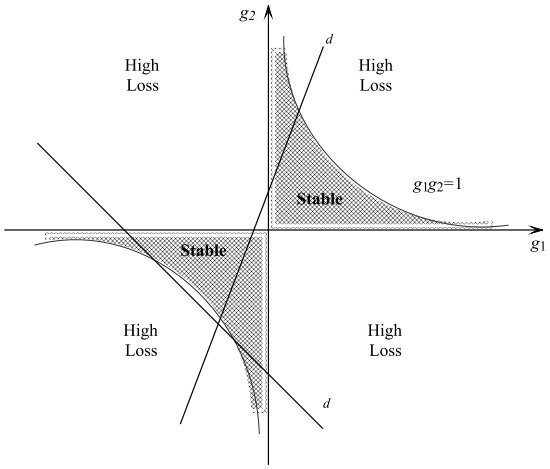

Fig. 5. Stability diagram.

The beam radius on gain medium ω_1, on M1 ω_2 and on M2 ω_3 can be expressed as [26]

$$\omega_1 = \sqrt{\frac{\lambda}{\pi} \frac{|2xu_1u_2 + u_1 + u_2|}{\left[(1-g_1g_2)g_1g_2\right]^{1/2}}} \tag{11}$$

$$\omega_2 = \sqrt{\frac{\lambda|L|}{\pi}\left[\frac{g_2}{g_1(1-g_1g_2)}\right]^{1/2}} \tag{12}$$

$$\omega_3 = \sqrt{\frac{\lambda|L|}{\pi}\left[\frac{g_1}{g_2(1-g_1g_2)}\right]^{1/2}}. \tag{13}$$

However, due to losses of the RBC system, the maximum transmission distance cannot be actually obtained. There are two kinds of loss influencing the transmission: the loss independent of the beam transverse mode, and the diffraction loss closely related to the transverse mode [20]. The former loss is determined by the system components, which is not related to the transmission distance. It can be taken as the leakage from the partially transparent mirror M2. On the contrary, the transverse mode related diffraction loss relies on the transmission distance.

2) Transmission Efficiency Modeling: The diffraction loss is mainly caused by the diffraction effect. According to [27], the resonant beam is formed by the interaction of resonant cavity and gain medium. When the resonant beam travels back and forth between M1 and M2, the edge of M1 and M2 will cause the diffraction loss because of the geometry of M1 and M2. To illustrate how to calculate the diffraction loss, it is useful to plot a stability diagram of stable resonant cavity. As shown in Fig. 6, a presents the radius of the end mirror M1 and M2 while $l + d$ presents the cavity length of the optical resonant cavity.

As shown in Fig. 6, after a number of round-trip propagations, the electric field distributions of the cross section of a resonant beam on the mirror M1 and M2 are $E_1(x, y)$, and $E_2(x, y)$. Then, there should be the following self-consistent relationship [27]:

$$E_2(x, y) = \gamma E_1(x, y) \tag{14}$$

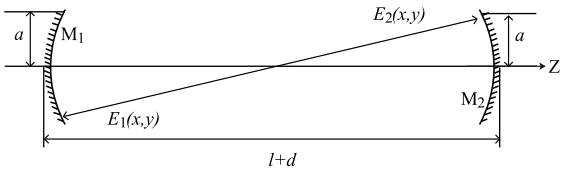

Fig. 6. Schematic of stable resonant cavity.

where γ is a complex constant factor, which reflects the change of amplitude and phase of beam field after a one-way propagation. The total energy loss of a single trip δ can be expressed as

$$\delta = \frac{|E_1|^2 - |E_2|^2}{|E_1|^2} = 1 - |\gamma|^2. \tag{15}$$

The losses independent of the beam transverse mode are related to the intrinsic properties of the components. Therefore, the losses independent of the beam transverse mode can be attributed to the reduction of reflectivity of partially transparent mirror M2. Thus, γ only contains the diffraction loss of the edge of the mirror M1 and M2. Normally, the diffraction loss is caused by the geometry of M1 and M2. Moreover, the diffraction loss is caused by the finite aperture in the resonant cavity, such as the aperture of gain medium. According to [28], the diffraction loss of the beam through an aperture, of which the diameter is $2a$, in the optical resonant cavity δ_{mn} is

$$\delta_{mn} = 1 - \frac{\int_0^{2\pi}\int_0^{a} r^{2m}\left[L_n^m(\frac{2r^2}{\omega^2})\right]^2 e^{-2\frac{r^2}{\omega^2}} r dr d\varphi}{\int_0^{2\pi}\int_0^{\infty} r^{2m}\left[L_n^m(\frac{2r^2}{\omega^2})\right]^2 e^{-2\frac{r^2}{\omega^2}} r dr d\varphi} \tag{16}$$

where m and n are positive integers, r is the radial radius, φ is the phase difference, and $L_n^m(\xi)$ is n order associative Laguerre polynomials.

For the general stable optical resonant cavity, the equivalent principle of the confocal resonator can be used to transform the diffraction loss [27]. In the RBC system, to improve the uniformity of beam cross section energy distribution, the resonant beam is the superposition of TEM_{00} mode and multiple higher order modes. The TEM_{00} presents the fundamental mode in an optical resonant cavity, which is inevitable in the resonant cavity. Since the order and quantity of higher order modes are difficult to be accurately predicted, the higher order modes are difficult to be analyzed. As the diffraction losses of the higher order modes are proportional to the TEM_{00} mode, we take the diffraction loss of TEM_{00} mode into consideration for simplicity. The total loss can be expressed as N times of the loss of TEM_{00} mode [20]. The diffraction loss of TEM_{00} mode $\delta_{00}(d)$, which is related to d, can be presented as

$$\delta_{00}(d) = e^{-2\pi\frac{a^2}{\lambda(l+d)}}. \tag{17}$$

The total diffraction loss is

$$\delta(d) = Ne^{-2\pi\frac{a^2}{\lambda(l+d)}} \tag{18}$$

where N is the ratio of total diffraction loss to diffraction loss $\delta_{00}(d)$.

To sum up, if the gain medium and the structure of the resonant cavity are given, the external-cavity beam power P_{beam} can be stimulated by the gain medium stored energy per second P_{stored}. The relationship between P_{beam} and P_{stored} can be depicted as

$$P_{\mathrm{beam}} = f(d)P_{\mathrm{stored}} + C \tag{19}$$

where $f(d)$ is the equation related to the transmission distance d, and C is a constant which depends on the internal parameters of the system.

With reference to (17) and [19], $f(d)$, which is closely related to the diffraction loss δ, can be computed as

$$\begin{aligned} f(d) &= \frac{2(1-R)m}{(1+R)\delta(d) - (1+R)\ln R} \\ &= \frac{2(1-R)m}{(1+R)Ne^{-2\pi\frac{a^2}{\lambda(l+d)}} - (1+R)\ln R} \end{aligned} \tag{20}$$

where R is the effective reflectivity of the partially transparent mirror M2. In this paper, R is related to the losses, which are independent of transmission distance, and m is the overlap efficiency.

Therefore, we can obtain the stored energy to beam power transmission efficiency η_{trans}

$$\eta_{\mathrm{trans}} = \frac{P_{\mathrm{beam}}}{P_{\mathrm{stored}}} = f(d) + \frac{C}{P_{\mathrm{stored}}}. \tag{21}$$

C. Beam Power-to-Electrical Power Conversion

In the RBC receiver, the external-cavity beam power can be converted to electrical power, which can be used to charge devices accessed to the RBC system. For certain input beam power, the output electrical power will be different if with different loads in the circuit. To obtain the maximum beam power to electrical power conversion efficiency, the PV-panel should work at the maximum output power state with the assistance of maximum power point tracking technology. As stated in [17], the maximum PV-panel output power P_{pv} takes a linear relationship with the external-cavity beam power P_{beam}, which is as

$$P_{\mathrm{pv}} = a_1 P_{\mathrm{beam}} + b_1. \tag{22}$$

Therefore, the beam power-to-electrical power conversion efficiency, i.e., the PV-panel conversion efficiency, η_{pv} depends on P_{pv} and P_{beam}, which can be depicted as

$$\eta_{\mathrm{pv}} = \frac{P_{\mathrm{pv}}}{P_{\mathrm{beam}}} = a_1 + \frac{b_1}{P_{\mathrm{beam}}}. \tag{23}$$

In summary, the PV-panel converts the received beam power P_{beam} to the output electrical power P_{pv} with the conversion efficiency η_{pv}.

D. End-to-End Power Transmission

Based on the above theoretical analysis for each procedure, the end-to-end power relationship, that is the relationship

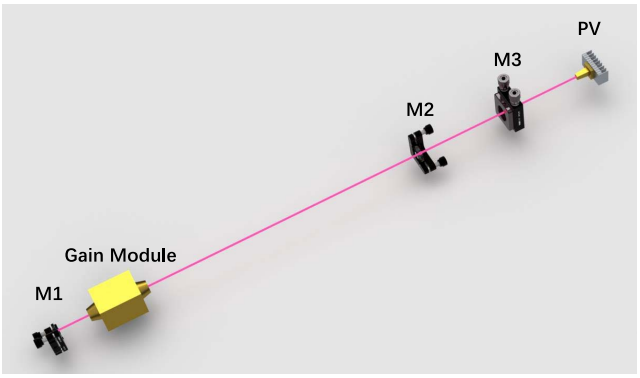

Fig. 7. Testbed schematic.

TABLE I
TRANSMISSION OR CONVERSION EFFICIENCY

Parameter	Description
η_{stored}	electrical power to gain medium stored energy conversion efficiency
η_{trans}	gain medium stored energy to external-cavity beam power transmission efficiency
η_{pv}	external-cavity beam power to electrical power conversion efficiency
η_{all}	end-to-end transmission efficiency

between the input electrical power and the output electrical power, can be depicted as

$$\begin{aligned} P_{\text{out}} &= a_1[f(d)P_{\text{stored}} + C] + b_1 \\ &= a_1 f(d)\eta_{\text{stored}}P_{\text{in}} + a_1 C + b_1. \end{aligned} \tag{24}$$

As can be seen, the system output power P_{out} is affected by the input power P_{in} and the transmission distance d. Based on (24), the relationship between the end-to-end transmission efficiency η_{all} and the input electrical power can be obtained as

$$\begin{aligned} \eta_{\text{all}} &= \eta_{\text{stored}}\eta_{\text{trans}}\eta_{\text{pv}} \\ &= a_1\eta_{\text{stored}}\eta_{\text{trans}} + \frac{b_1}{P_{\text{in}}} \\ &= a_1\eta_{\text{stored}}f(d) + \frac{a_1 C + b_1}{P_{\text{in}}}. \end{aligned} \tag{25}$$

As can be seen, η_{all} is affected by both P_{in} and d.

The transmission or conversion efficiency of each module and the RBC power transmission efficiency are listed in Table I.

The analytical model of the RBC energy transmission is illustrated, and the factors influencing the energy transmission are analyzed in this section. On this basis, the validation of theoretical model and the evaluation of the RBC system will be presented in the next section.

IV. VALIDATION AND EVALUATION

Based on the analytical model in the previous section, we can obtain that the RBC system efficiency varies with the input electrical power, the electrical power to stored energy conversion efficiency, the specifications of the gain medium, the transmission distance, the reflectivity of the mirrors, the overlap efficiency, the diffraction loss of the intracavity beam,

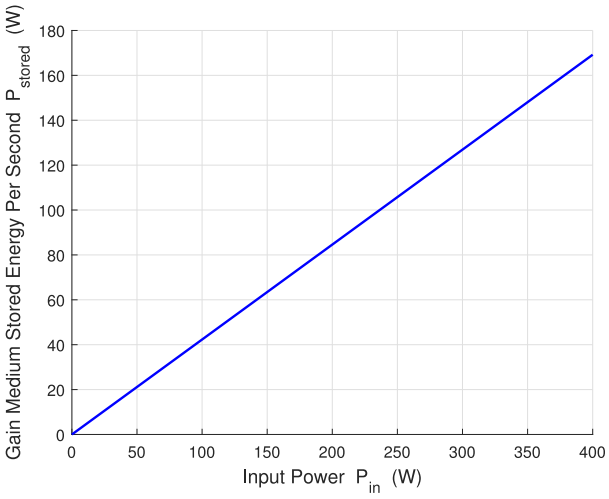

Fig. 8. Gain medium stored energy per second versus input power.

and the beam power to the electrical power conversion efficiency. In this section, we will introduce the RBC testbed at first. According to the measured data, we will validate the parameters of our theoretical model. Then, we will evaluate both the experimental and theoretical performance of the RBC system. Theoretical evaluations are implemented in MATLAB and Simulink.

A. RBC System Testbed

We establish the testbed of the RBC system which integrates the gain medium, the heat sinks, and the pump source in the gain module. The diagram of the testbed is shown in Fig. 7.

On the testbed, we take a rod-shape gain medium. Both end facets of the rod are antireflection coated at about 1 um. The doping concentration is chosen to be 0.6%. The gain medium is mounted with the water-cooled copper heat sinks, which allow efficient heat removal. The pump source is made of semiconductor laser diodes, of which the wavelength is 808 nm. The gain medium is side pumped by the pump source.

The resonant cavity consists of two curved mirrors M1 and M2. M1 is high-reflectivity coated at about 1 um. M2 is used as the output coupler with 88% reflectivity. The distance between M1 and M2 and the curvature of the two mirrors are determined by the stability condition introduced in Section III.

The PV-panel is constituted of vertical multijunction PV cell. The PV-panel with a heatsink can sustain 10 W beam power at maximum. To match the size of the PV-panel, the spot size of the external-cavity beam should be adjusted. The mirror M3 in Fig. 7 plays the role. M3 is a plano-convex lens with a focal length of 40 mm.

B. Electrical Power-to-Stored Energy Conversion

In the RBC transmitter, the input electrical power P_{in} is converted to the gain medium stored energy per second P_{stored}. The conversion efficiency is determined by the performance of pump source, the structure of the pump chamber and the material and size of the gain medium. From our measured

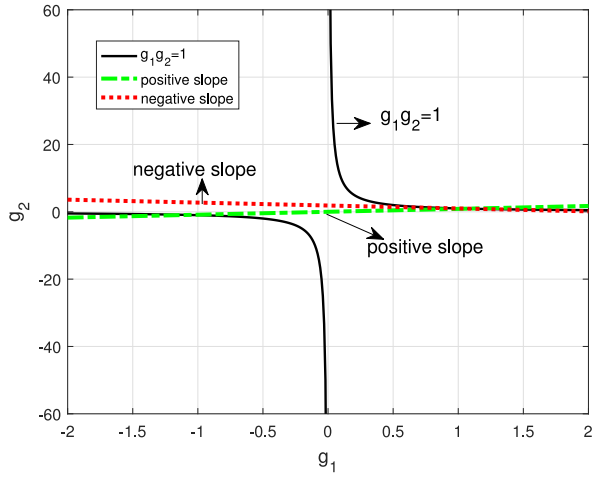

Fig. 9. Connected stability diagram.

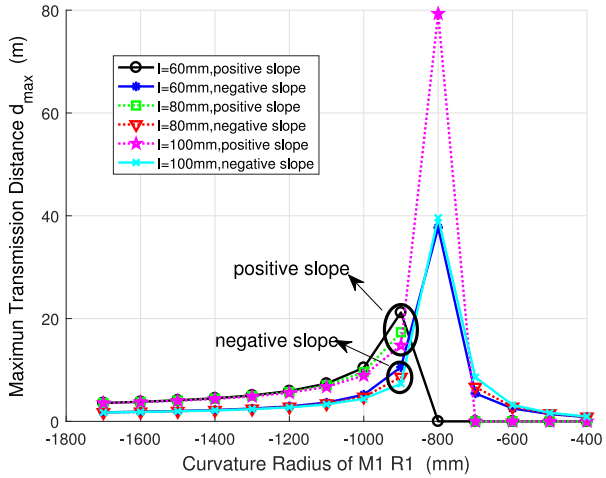

Fig. 10. Maximum transmission distance versus curvature radius of M1.

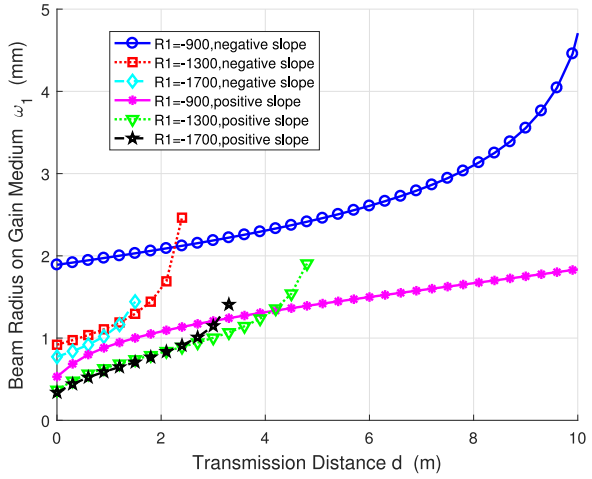

Fig. 11. Beam radius on gain medium versus transmission distance.

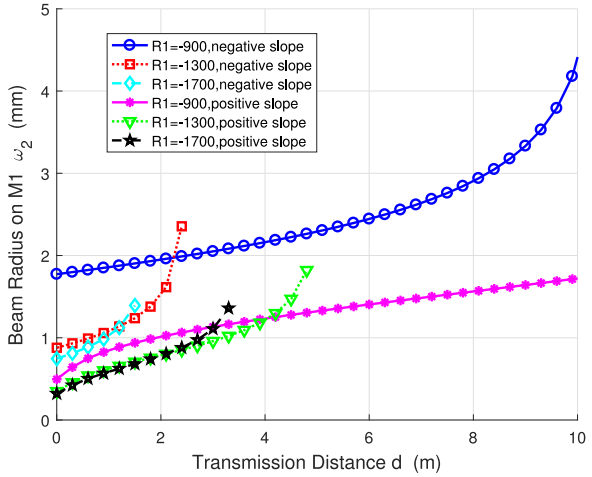

Fig. 12. Beam radius on M1 versus transmission distance.

data, we can conduct that the electrical power to stored energy conversion efficiency η_{stored} is 42.3%.

With reference to (1), the relationship between P_{stored} and P_{in} can be depicted out, as shown in Fig. 8. As can be seen, P_{stored} goes up linearly as P_{in} increases, and the straight line between P_{stored} and P_{in} passes through the origin.

C. Stored Energy-to-Beam Power Transmission

In this part, we will illustrate how to design the cavity structure and select the transmission distance, and how the transmission distance influences the stored energy to beam power transmission efficiency.

1) Transmission Distance Modeling: According to (3)–(5) and (7), given resonant cavity configuration, i.e., given l, f, R_1, and R_2, the position of a straight line in Fig. 5 is determined. The focal length f of Nd materials ranges from a few meters to tens of centimeters [19]. We set up $f = 880$ mm according to the results of experimental measurements. According to the geometric parameters of the gain medium used in practice, the shortest l is 60 mm. Then, we can obtain two distinct stability zones, as shown in Fig. 5. In an ideal wireless power transmission device, power is expected to be transmitted over any distances within the maximum transmission range. Thus, we expect the transmission range to be continuous, that is, the two stability regions are connected.

To achieve a continuous transmission distance, that is, to connect the two stability regions, the straight line in Fig. 5, which represents a cavity configuration, needs to satisfy the following condition. The intersection points of the straight line and the coordinate axis are coincident or the intersection points of the straight line and the $g_1g_2 = 1$ curve are coincident. There are two situations: 1) the straight line slope is positive, and through the origin and 2) the straight line slope is negative and tangent to $g_1g_2 = 1$. Fig. 9 shows the two situations that can connect two stability regions. The dashed line is with positive slope and the dotted one with negative slope. We can find that every set of values of $R1$ and l has two $R2$ solutions, which are corresponding to the two cases in Fig. 9.

Given l and $R1$, the maximum transmission distance $d_{\max}$ takes different values. The relationships among l, $R1$ and $d_{\max}$ for the two solutions are given in Fig. 10. When $R1 = -800$ mm, the solution of the negative slope about maximum transmission distance reaches the maximum value which is about 40 m. The maximum of positive slop is about 80 m.

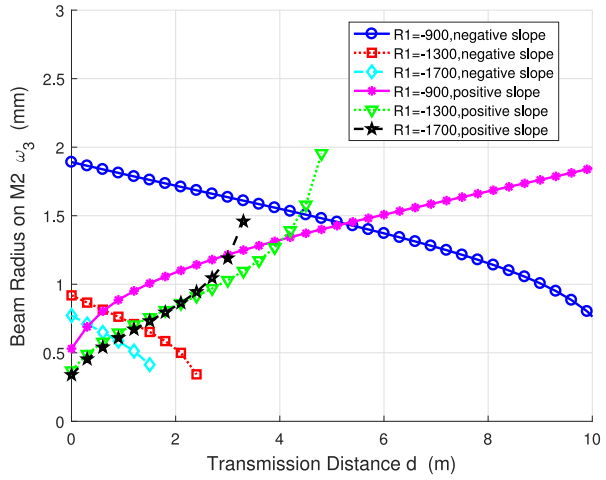

Fig. 13. Beam radius on M2 versus transmission distance.

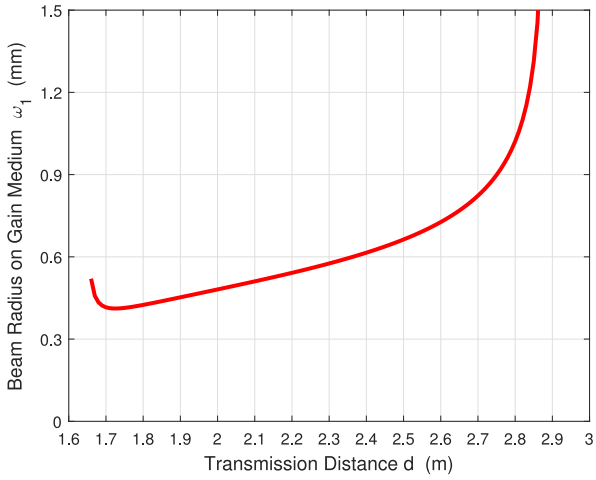

Fig. 14. Beam radius on gain medium versus transmission distance.

When $R1 < -900$ mm, the maximum transmission distance of the solution with the positive slope is larger than that solution with the negative slope. When l takes 60, 80, and 100 mm, the maximum transmission distance is slightly different.

Therefore, the beam transmission distance d can take any value lower than $d_{\max}$. However, with the variation of d, the beam radius on gain medium ω_1, on M1 ω_2, and on M2 ω_3 take different value. Based on (4), (5), and (11)–(13), how ω_1, ω_2, ω_3 change as d varies when l takes 60 mm is given in Figs. 11–13, respectively.

As can be seen, in the case of positive slope, the beam radius on gain medium ω_1, on M1 ω_2 and on M2 ω_3 increase with the increment of transmission distance. However, in the case of negative slope, the beam radiuses ω_1, ω_2 increase with the increment of transmission distance, while the beam radius ω_3 is the opposite. If with the same $R1$, the beam radiuses ω_1 and ω_2 are smaller in the case of positive slope than that of negative slope.

The beam radius on gain medium determines the cross-sectional size of the gain medium, and the price of the gain medium is determined by the size. In addition, the size of the gain medium affects the transmitter's size. For practical applications, the transmitter should be as smaller as possible.

Therefore, to make the transmission range of an RBC system continuous, the curvature radius of M1, M2 and the size of the gain medium are strictly required. In our testbed, M1 is a plane mirror, and M2 is a curved mirror, of which the curvature radius of M2 $R2$ is 2000 mm. The distance between M1 and the gain medium l is 250 mm.

Based on the theoretical model, how ω_1 changes as the transmission distance d varies is shown in Fig. 14. As shown, the effective range of d, which refers to the maximum energy transmission distance, varies from 1.65 to 2.85 m.

As shown in Fig. 14, the maximum and minimum beam radius on gain medium are about 1.5 and 0.4 mm, respectively. ω_1 decreases as d increases until reaches the minimum value. Then ω_1 increases as d increases. When d reaches 2.85 m, the ω_1 is up to 1.5 mm, which is equal to the radius of gain medium. The measured permitted range of energy transfer varies from 1.675 to 2.6 m, which is slightly different from the simulated results due to the system loss.

2) Transmission Efficiency Modeling: Based on the above analysis, the transmission distance and the structure of the resonant cavity are determined.

We measure the external-cavity beam power P_{beam} and the transmission efficiency η_{trans}, when transmitting the input power P_{in} over 2 m. The measured data is shown as the discrete points in Fig. 15. As shown, the threshold of gain medium stored energy per second to external-cavity beam power conversion is 75 W. When P_{stored} is over the threshold, P_{beam} increases as P_{stored} increases. η_{trans} goes up dramatically at first, and then the growing trend becomes slow. The maximum P_{beam} is 58 W and η_{trans} can be up to about 35% when P_{stored} takes 163 W.

From (19) and (20), given d, the function $f(d)$ becomes a constant, so P_{beam} linearly depends on P_{stored}. According to our measured data and [19], the effective reflectivity R of the mirror M2 in the receiver is 0.2618, the overlap efficiency m is 1 and C takes -51.83 in our theoretical model.

To numerically evaluate the relationship between P_{beam} and P_{stored}, we set d with 2 m. The relationship is shown as the linear line in Fig. 15. For the same d, the stored energy to the beam power conversion efficiency η_{trans} can be obtained according to (21). The relationship between η_{trans} and P_{stored} is given as the nonlinear curve in Fig. 15. As can be seen, the curves of theoretical calculation coincide with the changing trend of measured data.

From (19) and (21), given P_{stored}, $f(d)$ only varies with the transmitting distance d, thus P_{beam} relies on d. We measure how P_{beam} and η_{trans} change with d, when P_{stored} takes 89 W. The measured data is shown as the discrete points in Fig. 16. As can be seen, if P_{stored} is 89 W, P_{beam} is 10.18 W, and η_{trans} is 11.45% when $d = 1.675$ m, while P_{beam} is 6.88 W and η_{trans} is about 7.7% when $d = 2.6$ m. When d takes small values at first, P_{beam} goes down slowly. Then, as d goes up, P_{beam} goes down faster. While, the changing trend of η_{trans} over d is similar to that of P_{beam} when P_{stored} takes the same value.

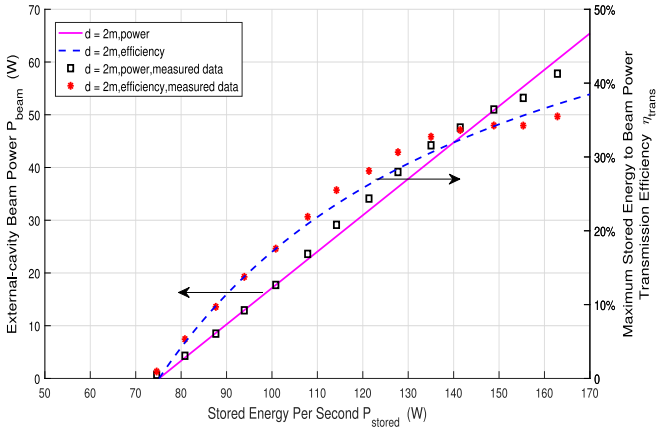

Fig. 15. Beam power and transmission efficiency versus stored energy per second.

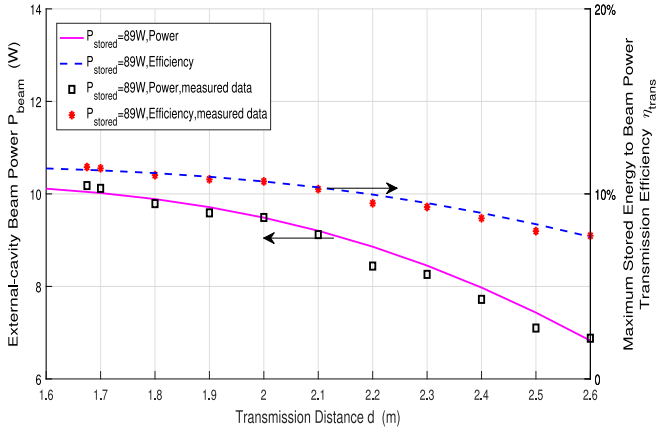

Fig. 16. Beam power and transmission efficiency versus transmission distance.

According to the measured data, N in (20) takes 13. Curves in Fig. 16 depict how P_{beam} and η_{trans} theoretically change with d, when P_{stored} takes 89 W. As can be seen, the theoretical curves fit the measured data well. This illustrates that our theoretical model coincides with the experimental results.

Part of the gain medium stored energy that is not converted to the resonant beam is scattered into the environment. However, the scattered power is with low density, so safety of the system can be guaranteed.

D. Beam Power-to-Electrical Power Conversion

In the RBC receiver, the PV-panel takes the role of converting the external-cavity beam power to the electrical power. The discrete points in Fig. 17 represent the measured maximum PV-panel output power with different received external-cavity beam power. As shown, when the received beam power P_{beam} is 9.07 W and η_{pv} takes 17.22%, P_{pv} can be up to about 1.562 W. The PV-panel can sustain 10 W beam power at maximum due to the limitations of the material and the cooling effect. With the help of the measured data and Simulink, theoretical values of a_1 and b_1 in (22) are 0.3487 and -1.535, respectively.

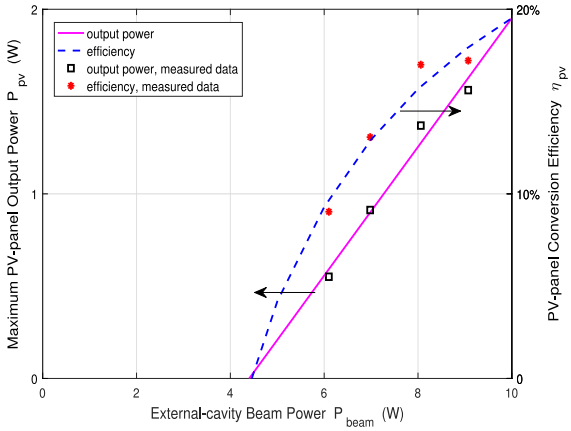

Fig. 17. PV-panel output power and conversion efficiency versus beam power.

Thus, we can obtain the relationship between the maximum PV-panel output power P_{pv} and the received external-cavity beam power P_{beam}, which is shown as the linear line in Fig. 17. Since only after accumulating a certain amount of energy can the PV-panel convert the external-cavity beam power to the electrical power, there is a threshold before the electrical power is output. After P_{beam} becomes larger than the threshold, P_{pv} increases over P_{beam}.

Thereafter, the relationship between the PV-panel efficiency η_{pv} and P_{beam} can be obtained, which is shown as the nonlinear curve in Fig. 17. After P_{beam} is over the threshold, η_{pv} goes up dramatically as P_{beam} increases. Then, η_{pv} increases more slowly, and the maximum value of η_{pv} is about 19.5% when P_{beam} is 10 W.

E. End-to-End Power Transmission

Based on the above analysis, the end-to-end power transmission procedure, that is the whole RBC charging system energy transmission procedure, can be depicted. The end-to-end power relationship, that is the relationship between the input electrical power for driving the system and the output electrical power for charging devices, can be obtained. Based on (24), when the transmission distance d takes 2 m, the end-to-end power takes a linear relationship, which can be depicted as the linear line in Fig. 18. As stated above, there are thresholds of the stored energy to the beam power transmission and the beam power to the electrical power conversion, and there is a threshold in the end-to-end power conversion relationship. After exceeding the threshold, P_{out} goes up linearly as P_{in} increases.

Then, how the end-to-end power transmission efficiency η_{all} changes over P_{in} can be obtained. The nonlinear curve in Fig. 18 depicts the relationship between η_{all} and P_{in}. η_{all} goes up gradually with the increment of P_{in} after that P_{in} is over the threshold. From Fig. 18, we can obtain how much input power should be provided if we want to charge devices with certain power at certain distance. For example, if we want to charge our devices with 2 W over 2 m, the input power to the transmitter should be about 213 W. The corresponding end-to-end efficiency is about 0.94% under this condition.

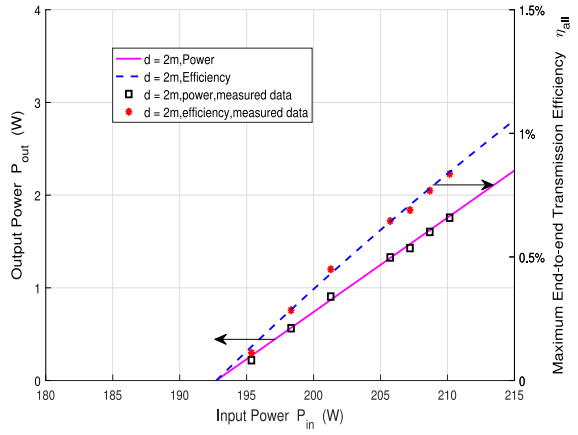

Fig. 18. Output power and transmission efficiency versus input power.

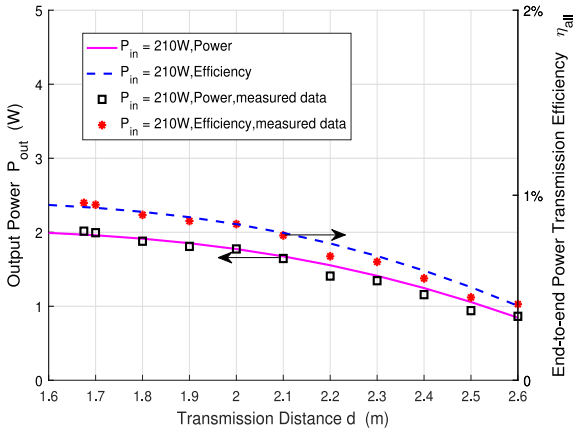

Fig. 19. Output power and transmission efficiency versus transmission distance.

The discrete points in Fig. 18 represent the measured data. To avoid damage to the PV-panel, the maximum input power is set as 210 W. If d takes 2 m, P_{out} can be up to about 1.76 W and η_{all} is 0.8%. The measured data matches well with the theoretical results.

On the other hand, for certain P_{in}, the changing trend among P_{out}, η_{all}, and d can be depicted. Fig. 19 gives all the relationships when P_{in} takes 210 W. P_{out} goes down slowly when d is relatively short. With the increment of d, P_{out} goes down dramatically. The changing trend of η_{all} over d is similar to that of P_{out} when P_{in} takes the same value. As d increases, η_{all} decreases more and more dramatically.

When d is 1.675 m, P_{out} can be up to about 2 W and η_{all} is 0.96%. When d increases to 2.6 m, P_{out} is about 0.86 W and η_{all} is 0.41%. Figs. 18 and 19 provide guidelines for the power and efficiency control and the distance selection when designing and implementing the RBC system.

To conclude, the factors influencing the overall RBC efficiency include the input electrical power, the electrical power to stored energy conversion efficiency, the transmission distance, and the PV-panel conversion efficiency. The maximum transmission distance is determined by the stability condition of the optical resonant cavity, the material and size of the gain medium, the diameter of the transmitter and the receiver, and the diffraction loss. To summarize:

1) we obtain the maximum RBC transmission distance;
2) we analyze the factors influencing the energy transmission, and give the energy attenuation model;
3) we establish an RBC testbed and validate the parameters of our theoretical model;
4) we evaluate both the experimental and theoretical performance of the RBC system;
5) we derive the end-to-end RBC efficiency model, which provides guidelines for the RBC system design and deployment.

V. Conclusion

To provide perpetual power supply to IoT devices, RBC is a promising safe, long-range, and high-power WPT solution. In this paper, we present the analytical model of the energy transmission channel for the RBC system, and study how long distance RBC can reach and how much power RBC can transfer in theory. Based on the theoretical model, we establish a testbed of the RBC system. The experiments verify that the RBC transmitter can provide up to 2 W electrical power to the RBC receiver. The maximum energy transmission distance is 2.6 m. Parameters of the theoretical model are validated based on the measured data. Both the experimental and theoretical performance of the RBC system are evaluated in terms of the transmission distance, the transmission efficiency, and the output electrical power. The theoretical model and the experimental testbed lead to guidelines for the RBC system design and implementation in practice.

There are some open issues to be studied in future work.

1) Since there are other losses influencing the RBC efficiency in addition to the diffraction loss. How to improve the overall RBC efficiency needs to be further investigated.
2) Performance of the RBC system is affected by other factors such as the temperature. The stability and reliability of the RBC system need further investigation.

Acknowledgment

The authors would like to thank H. Deng and M. Xiong for their inputs on the experiment and would also like to thank the anonymous reviewers for their valuable comments and suggestions to improve the quality of this paper.

References

[1] Y. Zhou, C. Huang, T. Jiang, and S. Cui, "Wireless sensor networks and the Internet of Things: Optimal estimation with nonuniform quantization and bandwidth allocation," *IEEE Sensors J.*, vol. 13, no. 10, pp. 3568–3574, Oct. 2013.

[2] T. Chen, Y. Shen, Q. Ling, and G. B. Giannakis, "Online learning for 'thing-adaptive' fog computing in IoT," in *Proc. ASILOMAR*, Pacific Grove, CA, USA, Oct./Nov. 2017, pp. 664–668.

[3] Q. Wu *et al.*, "Cognitive Internet of Things: A new paradigm beyond connection," *IEEE Internet Things J.*, vol. 1, no. 2, pp. 129–143, Apr. 2014.

[4] S. Yu, M. Liu, W. Dou, X. Liu, and S. Zhou, "Networking for big data: A survey," *IEEE Commun. Surveys Tuts.*, vol. 19, no. 1, pp. 531–549, 1st Quart., 2017.

[5] A. Carroll and G. Heiser, "An analysis of power consumption in a smartphone," in *Proc. USENIX Conf. USENIX Annu. Tech. Conf.*, Jun. 2010, p. 21.
[6] K. Georgiou, S. Xavier-de-Souza, and K. Eder, "The IoT energy challenge: A software perspective," *IEEE Embedded Syst. Lett.*, vol. 10, no. 3, pp. 53–56, Sep. 2018.
[7] S. Yu, W. Zhou, S. Guo, and M. Guo, "A feasible IP traceback framework through dynamic deterministic packet marking," *IEEE Trans. Comput.*, vol. 65, no. 5, pp. 1418–1427, May 2016.
[8] H. Zhang, Y. Qiu, X. Chu, K. Long, and V. C. M. Leung, "Fog radio access networks: Mobility management, interference mitigation, and resource optimization," *IEEE Wireless Commun.*, vol. 24, no. 6, pp. 120–127, Dec. 2017.
[9] X. Lu, D. Niyato, P. Wang, D. I. Kim, and Z. Han, "Wireless charger networking for mobile devices: Fundamentals, standards, and applications," *IEEE Wireless Commun.*, vol. 22, no. 2, pp. 126–135, Apr. 2015.
[10] S. S. Valtchev, E. N. Baikova, and L. R. Jorge, "Electromagnetic field as the wireless transporter of energy," *Facta Universitatis Electron. Energetics*, vol. 25, no. 3, pp. 171–181, Dec. 2012.
[11] B. L. Cannon J. F. Hoburg, D. D. Stancil, and S. C. Goldstein, "Magnetic resonant coupling as a potential means for wireless power transfer to multiple small receivers," *IEEE Trans. Power Electron.*, vol. 24, no. 7, pp. 1819–1825, Jul. 2009.
[12] Z. Popovic, "Cut the cord: Low-power far-field wireless powering," *IEEE Microw. Mag.*, vol. 14, no. 2, pp. 55–62, Mar./Apr. 2013.
[13] J. Fakidis, S. Videv, H. Helmers, and H. Haas, "0.5-Gb/s OFDM-based laser data and power transfer using a GaAs photovoltaic cell," *IEEE Photon. Technol. Lett.*, vol. 30, no. 9, pp. 841–844, May 1, 2018.
[14] A. Sahai and D. Graham, "Optical wireless power transmission at long wavelengths," in *Proc. Int. Conf. Space Opt. Syst. Appl. (ICSOS)*, Santa Monica, CA, USA, May 2011, pp. 164–170.
[15] Q. Liu *et al.*, "Charging unplugged: Will distributed laser charging for mobile wireless power transfer work?" *IEEE Veh. Technol. Mag.*, vol. 11, no. 4, pp. 36–45, Dec. 2016.
[16] Q. Zhang *et al.*, "Distributed laser charging: A wireless power transfer approach," *IEEE Internet Things J.*, vol. 5, no. 5, pp. 3853–3864, Oct. 2018.
[17] Q. Zhang *et al.*, "Adaptive distributed laser charging for efficient wireless power transfer," in *Proc. IEEE 86th Veh. Technol. Conf. (VTC-Fall)*, Toronto, ON, Canada, Sep. 2017, pp. 1–5.
[18] Q. Zhang *et al.*, "Adaptive resonant beam charging for intelligent wireless power transfer," *IEEE Internet Things J.*, to be published. doi: 10.1109/JIOT.2018.2867457.
[19] W. Koechner, *Solid-State Laser Enegineering*. Beijing, China: Sci. Press, 2002.
[20] S. Cao *et al.*, "Analysis of diffraction loss in laser resonator," *Laser Technol.*, vol. 42, no. 3, pp. 400–403, Sep. 2018.
[21] M. S. Aziz, S. Ahmad, I. Husnaini, A. Hassan, and U. Saleem, "Simulation and experimental investigation of the characteristics of a PV-harvester under different conditions," in *Proc. Int. Conf. Energy Syst. Policies*, Nov. 2014, pp. 1–8.
[22] M. A. Green, K. Emery, Y. Hishikawa, W. Warta, and E. D. Dunlop, "Solar cell efficiency tables (version 45)," *Progr. Photovolt. Res. Appl.*, vol. 23, no. 1, pp. 1–9, 2015.
[23] L. Summerer and O. Purcell, "Concepts for wireless energy transmission via laser," in *Proc. Int. Conf. Space Opt. Syst. Appl.*, 2008, pp. 1–10.
[24] H. Kogelnik, "Imaging of optical modes—Resonators with internal lenses," *Bell Syst. Tech. J.*, vol. 44, no. 3, pp. 455–494, Mar. 1965.
[25] H. Kogelnik and T. Li, "Laser beams and resonators," *Appl. Opt.*, vol. 5, no. 10, pp. 1550–1567, Oct. 1966.
[26] V. Magni, "Resonators for solid-state lasers with large-volume fundamental mode and high alignment stability," *Appl. Opt.*, vol. 25, no. 1, pp. 107–117, Jan. 1986.
[27] B. Zhou, Y. Gao, and J. Chen, *Laser Principle*, 6th ed. Beijing, China: Nat. Defense Press, 2004.
[28] G. Wei and B. Zhu, *Laser Beam Optics*, 1st ed. Beijing, China: Beijing Ind. Collage Press, 1988.

Authors' photographs and biographies not available at the time of publication.